DALTON

Dinuclear complexes of Mn^{II}, Co^{II} and Zn^{II} triply bridged by carboxylate groups: structures, properties and catalase-like function‡

Masako Yamami, Megumi Tanaka, Hiroshi Sakiyama,*,† Takeichiro Koga, Kensuke Kobayashi, Hitoshi Miyasaka, Masaaki Ohba and Hisashi Ōkawa*

Department of Chemistry, Faculty of Science, Kyushu University, Hakozaki, Higashiku, Fukuoka 812, Japan

1,3-Bis[(2-dimethylaminoethyl)iminomethyl]benzene (baib), having two isolated metal-binding sites separated by a *m*-xylenylene group, formed dinuclear metal(II) complexes $[Mn_2(baib)(O_2CPh)_3]BPh_4$·MeCN **1**, $[Mn_2(baib)(O_2CPh)_3(NCS)]$ **2**, $[Co_2(baib)(O_2CMe)_3]BPh_4$ **3**, $[Co_2(baib)(O_2CPh)_3]BPh_4$ **4** and $[Zn_2(baib)(O_2CMe)_3]BPh_4$ **5**. The structure of a dimethylformamide adduct of **2**, $[Mn_2(baib)(O_2CPh)_3(NCS)]$·dmf **2′**, was determined. It has a dinuclear core bridged by two benzoate groups in the symmetric $\eta^1:\eta^1$ mode and one benzoate group in the asymmetric $\eta^1:\eta^2$ mode, with a Mn · · · Mn separation of 3.501(4) Å. A thiocyanate ion co-ordinates to one Mn through its nitrogen; both manganese ions are six-co-ordinated. Complex **3** was also characterized crystallographically. The pair of cobalt ions are bridged by three acetate groups in the $\eta^1:\eta^1$ mode with a Co · · · Co intermetallic separation of 3.449(2) Å. The geometry about each Co is a trigonal bipyramid. The complexes **4**·MeCN (**4′**) and **5** have dinuclear cores essentially similar to that of **3**: Co · · · Co 3.482(2) and Zn · · · Zn 3.4648(7) Å. The physicochemical properties of the complexes are reported together with the catalase-like function of **1**–**3**.

Dinuclear metal cores are versatile in biological systems[1] and model studies of bimetallic biosites by use of simple metal complexes are becoming important. Dinuclear cores bridged by one oxygen-containing (oxo, hydroxo or water) and one or two carboxylate groups are widely known in biosites such as haemerythrin,[2] ribonucleotide reductase,[3] phospholipase C,[4] *etc.* A similar dinuclear core is proposed for the active site of manganese catalase (MnCAT).[5] Phenol-based compartmental ligands of 'end-off' type, possessing two chelating arms attached to the 2 and 6 positions of the phenolic ring, have often been used to provide μ-phenoxo-bis(μ-carboxylato) dinuclear core complexes relevant to μ-oxo-bis(μ-carboxylato) cores. Our previous studies using such ligands have shown that μ-phenoxo-bis(μ-carboxylato)dimanganese core complexes act as functional models of MnCAT.[6–9]

Parallel to such 'end-off'-type ligands, dinucleating ligands with two metal-binding sites isolated by a spacer are also important, because they are expected to allow the involvement of an oxygen-containing bridge between a pair of metal ions. In this context 1,3-bis[(2-dimethylaminoethyl)iminomethyl]-benzene (baib) which has two isolated metal-binding sites separated by a *m*-xylenylene group is of interest. In this study the following dinuclear metal(II) complexes have been derived from baib: $[Mn_2(baib)(O_2CPh)_3]BPh_4$·MeCN **1**, $[Mn_2(baib)(O_2CPh)_3(NCS)]$ **2**, $[Co_2(baib)(O_2CMe)_3]BPh_4$ **3**, $[Co_2(baib)(O_2CPh)_3]BPh_4$ **4** and $[Zn_2(baib)(O_2CMe)_3]BPh_4$ **5**. Crystal structures, physicochemical properties and the catalase (CAT)-like function of the complexes are reported.

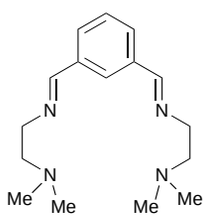

baib

Experimental

Measurements

Elemental analyses (C, H and N) were obtained at the Elemental Analysis Service Centre of Kyushu University. Analyses of Mn were obtained using a Shimadzu AA-660 atomic absorption/flame emission spectrophotometer. Infrared spectra were recorded on a JASCO IR-810 spectrometer using KBr discs or Nujol mulls. Molar conductances were measured at $\approx 1 \times 10^{-3}$ M concentration using a DKK AOL-10 conductivity meter at 20 °C. Electronic spectra were recorded using a Shimadzu MPS-2000 spectrometer. Magnetic susceptibilities were measured on a Faraday balance in the temperature range 80–300 K and on a HOXAN HSM-D SQUID susceptometer in the range 4.2–80 K. Calibrations were made using $[Ni(en)_3][S_2O_3]$ (en = ethane-1,2-diamine).[10] Diamagnetic corrections were made using Pascal's constants.[11] Cyclic voltammograms were recorded using a BAS CV-50W electrochemical analyser in dimethylformamide (dmf) or dimethyl sulfoxide (dmso) solution containing tetra(*n*-butyl)ammonium perchlorate as the supporting electrolyte. A three-electrode cell was used which was equipped with a glassy-carbon working electrode, a platinum coil as the counter electrode, and a $Ag–Ag^+$ ($NBu^n_4ClO_4$–acetonitrile) reference electrode. **CAUTION**: $NBu^n_4ClO_4$ is explosive and should be handled with great care.

Preparation

1,3-Bis[(2-dimethylaminoethyl)iminomethyl]benzene (baib). A solution of isophthalaldehyde (0.134 g, 1 mmol) and *N*,*N*-dimethylethane-1,2-diamine (0.176 g, 2 mmol) in toluene (30 cm^3) was heated for 3 h at the reflux temperature while the water resulting from the Schiff-base formation was eliminated azeotropically. On evaporating the reaction solution to dryness, crude baib was obtained as a yellow oily substance. It was used for the preparation of the following complexes without further purification.

† *Present address*: Department of Material and Biological Chemistry, Faculty of Science, Yamagata University, Yamagata 990, Japan.
‡ *Non-SI unit employed*: $\mu_B \approx 9.27 \times 10^{-24}$ J T^{-1}.

$[Mn_2(baib)(O_2CPh)_3]BPh_4$·MeCN 1. All the operations for syntheses were performed in an atmosphere of nitrogen to avoid oxidation from atmospheric dioxygen. To a methanolic solution (15 cm^3) of baib (0.137 g, 0.5 mmol) was added manganese(II) benzoate tetrahydrate (0.369 g, 1 mmol) and the mixture stirred at the reflux temperature for 20 min to form a yellow solution. The addition of sodium tetraphenylborate (0.342 g, 1 mmol) resulted in the precipitation of a pale yellow precipitate. It was recrystallized from acetonitrile as yellow crystals. Yield 0.265 g (47%) (Found: C, 68.1; H, 5.9; Mn, 10.0, N, 6.8. Calc. for $C_{63}H_{64}BMn_2N_5O_6$: C, 68.3; H, 5.8; Mn, 9.9; N, 6.3%). Selected IR ($\tilde{\nu}/cm^{-1}$) using KBr: 1640, 1565, 1404 and 700. μ_{eff} per Mn: 5.66 μ_B at 290 K. Molar conductance (Λ_M/S cm^2 mol^{-1}): 42 in CH_2Cl_2, 33 in dmf. UV/VIS [λ/nm (ε/M^{-1} cm^{-1})] in dmf: 275 (7300), 297 (1960) and 307 (1270).

$[Mn_2(baib)(O_2CPh)_3(NCS)]$ 2. This complex was obtained as a pale yellow precipitate in a way similar to that of **1**, except for the use of NaNCS instead of $NaBPh_4$. The yield was 0.261 g (31%) (Found: C, 56.0; H, 5.2; Mn, 13.1; N, 8.0. Calc. for $C_{40}H_{49}Mn_2N_5O_8S$: C, 55.9; H, 5.4; Mn, 13.1; N, 8.4%). Selected IR ($\tilde{\nu}/cm^{-1}$) using KBr: 2070, 1640, 1570, 1400 and 700. μ_{eff} per Mn: 5.75 μ_B at 290 K. Molar conductance (Λ_M/S cm^2 mol^{-1}): non-electrolyte in CH_2Cl_2, 58 in dmf. UV/VIS [λ/nm (ε/M^{-1} cm^{-1})] in dmf: 276 (5700), 295 (2310) and 306 (1420).

A portion was crystallized from a propan-2-ol–dmf mixture as a dmf adduct $[Mn_2(baib)(O_2CPh)_3(NCS)]$·dmf **2′** suitable for X-ray crystallography.

$[Co_2(baib)(O_2CMe)_3]BPh_4$ 3. A methanolic solution (10 cm^3) of baib (0.137 g, 0.5 mmol) and a methanolic solution of cobalt(II) acetate tetrahydrate (0.249 g, 1 mmol) were mixed and stirred at the reflux temperature for 3 h. The addition of sodium tetraphenylborate (0.342 g, 1 mmol) followed by further stirring at room temperature resulted in the precipitation of purple microcrystals. Yield 0.369 g (83%) (Found: C, 62.3; H, 6.2; Co, 13.7; N, 6.2. Calc. for $C_{46}H_{55}BCo_2N_4O_6$: C, 62.2; H, 6.2; Co, 13.3; N, 6.3%). FAB mass spectrum: *m/z* 596 for $[Co_2(baib)(O_2CMe)_3]^+$. Selected IR ($\tilde{\nu}/cm^{-1}$) using KBr: 1640, 1610 and 1440. μ_{eff} per Co: 4.2 μ_B at 290 K. Molar conductance (Λ_M/S cm^2 mol^{-1}): 52 in CH_2Cl_2. UV/VIS [λ/nm (ε/M^{-1} cm^{-1})]: 243 (33 900), 476 (77), 555 (95) and 780 (23) in CH_2Cl_2; 262 (17 600), 300 (2050), 498 (65) and 520 (70) in dmf.

$[Co_2(baib)(O_2CPh)_3]BPh_4$ 4. This complex was obtained as purple microcrystals in a way similar to that of **3** except for the use of cobalt(II) benzoate tetrahydrate. The yield was 0.279 g (52%) (Found: C, 67.9; H, 5.8; Co, 10.5; N, 5.2. Calc. for $C_{61}H_{61}BCo_2N_4O_6$: C, 68.2; H, 5.7; Co, 11.0; N, 5.2%). Selected IR ($\tilde{\nu}/cm^{-1}$) using KBr: 1640, 1600 and 1420. μ_{eff} per Co: 4.7 μ_B at 290 K. Molar conductance (Λ_M/S cm^2 mol^{-1}): 50 in CH_2Cl_2. UV/VIS [λ/nm (ε/M^{-1} cm^{-1})]: 245 (32 700), 485 (84), 557 (129), 772 (30) in CH_2Cl_2; 263 (18 000), 300 (2500), 500 (70) and 523 (77) in dmf.

A portion was recrystallized from acetonitrile as an acetonitrile adduct $[Co_2(baib)(O_2CPh)_3]BPh_4$·MeCN **4′** suitable for X-ray crystallography.

$[Zn_2(baib)(O_2CMe)_3]BPh_4$ 5. This complex was obtained as a colourless precipitate in a way similar to that of **3** using zinc(II) acetate dihydrate instead of cobalt(II) acetate tetrahydrate. The yield was 0.306 g (68%) (Found: C, 61.0; H, 6.2; N, 6.1; Zn, 14.5. Calc. for $C_{46}H_{55}BN_4O_6Zn_2$: C, 61.3; H, 6.2; N, 6.2; Zn, 14.5%). Selected IR ($\tilde{\nu}/cm^{-1}$) using KBr: 1650, 1620 and 1440. Molar conductance (Λ_M/S cm^2 mol^{-1}): 51 in CH_2Cl_2. UV/VIS [λ/nm (ε/M^{-1} cm^{-1})] in dmf: 262 (17 000) and 300 (2000). ^1H NMR ($CDCl_3$): δ 8.21 (s, 1 H), 7.88 (s, 2 H), 7.45 (m, 8 H), 7.40–7.33 (m, 3 H), 7.03 (t, 8 H), 6.87 (t, 4 H), 3.34 (t, 4 H), 2.55 (t, 4 H), 2.50 (s, 12 H) and 1.75 (s, 9 H).

Studies of catalase-like activity

A closed vessel containing a dmf solution (2 cm^3) of a dinuclear complex (5 μmol) was stirred at 0 °C on an ice–water bath. Hydrogen peroxide (10.0%, 0.5 cm^3; 1.45 mmol) chilled at 0 °C was injected through a silicon stopper and dioxygen evolved was measured volumetrically with a burette.

Crystallography

The complexes $[Mn_2(baib)(O_2CPh)_3(NCS)]$·dmf **2′**, $[Co_2(baib)(O_2CMe)_3]BPh_4$ **3**, $[Co_2(baib)(O_2CPh)_3]BPh_4$·MeCN **4′** and $[Zn_2(baib)(O_2CMe)_3]BPh_4$ **5** were subjected to crystallographic studies. Each single crystal of **2′**, **4′** and **5** was mounted on a glass fibre and coated with epoxy resin and a crystal of **3** was sealed in a glass tube. Intensity and lattice parameter measurements were made on a Rigaku AFC7R diffractometer with graphite-monochromated Mo-Kα radiation ($\lambda = 0.710\,69$ Å) and a 12 kW rotating-anode generator. The data were collected at 20 ± 1 °C using the ω–2θ scan technique to a maximum 2θ value of 50.0° for **2′**, **4′** and **5** and 45.0° for **3** at a scan speed 16.0° min^{-1} (in ω). The weak reflections [$I < 10.0\sigma(I)$] were rescanned up to a maximum of four scans and the counts were accumulated to ensure good counting statistics. Stationary background counts were recorded on each side of the reflection. The ratio of the peak counting time to the background counting time was 2:1. The cell parameters were determined by 25 reflections in the range $20.12 \leqslant 2\theta \leqslant 24.57°$ for **2′**, $20.03 \leqslant 2\theta \leqslant 24.79°$ for **3**, $28.77 \leqslant 2\theta \leqslant 29.85°$ for **4′** and $29.23 \leqslant 2\theta \leqslant 29.95°$ for **5**. The octant measured was $+h$, $+k$, $\pm l$ for all the complexes. The intensities of representative reflections were measured after every 150. Over the course of data collection the standards changed more or less and a linear correction factor was applied. Intensity data were corrected for Lorentz–polarization effects. Pertinent crystallographic parameters are summarized in Table 1.

The structures were solved by the direct method and expanded using the Fourier technique. The non-hydrogen atoms in complexes **3**, **4′** and **5** were refined anisotropically. Hydrogen atoms were included in the structure-factor calculations but not refined. In the case of **2** the fragile nature of the crystal precluded the improvement in quality of the structure analysis. For this complex the atoms of the dmf molecule were refined isotropically. Neutral atom scattering factors were taken from Cromer and Waber.[12] Anomalous dispersion effects were included in F_c; the values for $\Delta f'$ and $\Delta f''$ were those of Creagh and McAuley.[13] The values for the mass-attenuation coefficients were those of Creagh and Hubbell.[14] All calculations were performed using the TEXSAN crystallographic software package.[15]

CCDC reference number 186/728.

Results and Discussion

Crystal structures

$[Mn_2(baib)(O_2CPh)_3(NCS)]$·dmf 2′. An ORTEP[16] drawing of the essential part of complex **2′** is shown in Fig. 1 together with the numbering scheme. The relevant bond distances and angles are listed in Table 2.

The complex is depicted as $[Mn_2(baib)(O_2CPh)_3(NCS)]$; the dmf molecule is free from co-ordination and captured in the crystal lattice. The pair of manganese ions are bridged by two benzoate groups in the symmetric η^1:η^1 mode and one benzoate group in unsymmetric η^1:η^2 mode. Atom Mn(1) is six-co-ordinated with N(1) and N(2) of one pendant arm of baib, O(1) and O(2) of the chelating benzoate group and O(3) and O(6) of the two symmetrically bridging benzoate groups. The surroundings are largely distorted from a regular octahedron; the Mn–N and Mn–O bond distances vary from 2.00(2) to 2.38(2) Å.

Atom Mn(2) is also six-co-ordinated with N(3) and N(4) of the pendant arm of baib, O(1), O(4) and O(5) of the bridging

Table 1 Pertinent crystallographic parameters for complexes **2′**, **3**, **4′** and **5**

	2′	**3**	**4′**	**5**
Formula	$C_{41}H_{48}Mn_2N_6O_7S$	$C_{46}H_{55}BCo_2N_4O_6$	$C_{63}H_{64}BCo_2N_5O_6$	$C_{46}H_{55}BN_4O_6Zn_2$
M	878.80	888.64	1115.90	901.53
Crystal colour	Yellow	Purple	Purple	Colourless
Crystal system	Monoclinic	Monoclinic	Monoclinic	Monoclinic
Space group	$P2_1$	$P2_1/n$	$P2_1/c$	$P2_1/c$
a/Å	9.047(3)	15.500(3)	11.553(6)	15.119(2)
b/Å	16.305(5)	15.178(7)	17.375(5)	21.201(3)
c/Å	14.759(2)	20.411(8)	29.288(7)	15.456(1)
β/°	97.97(2)	106.89(2)	98.41(4)	108.186(8)
U/Å^3	2156.1(9)	4594(3)	5815(3)	4706.6(8)
Z	2	4	4	4
D_c/g cm^{-3}	1.354	1.285	1.274	1.272
μ(Mo-Kα)/cm^{-1}	6.88	7.72	6.25	10.68
No. of reflections	4226	6574	11 174	8958
R^a	8.7	5.6	5.1	5.0
R'^b	9.6	5.7	5.3	3.6

^{a} $\Sigma||F_o| - |F_c||/\Sigma|F_o|$. ^{b} $[\Sigma w(|F_o| - |F_c|)^2/\Sigma w|F_o|^2]^{\frac{1}{2}}$, $w = 1/\sigma(F_o)^2$.

Table 2 Relevant bond distances (Å) and angles (°) for complex **2′**

Mn(1)–N(1)	2.38(2)	Mn(2)–N(3)	2.27(2)
Mn(1)–N(2)	2.28(2)	Mn(2)–N(4)	2.35(3)
Mn(1)–O(1)	2.28(1)	Mn(2)–N(5)	2.16(2)
Mn(1)–O(2)	2.25(2)	Mn(2)–O(1)	2.25(2)
Mn(1)–O(3)	2.08(2)	Mn(2)–O(4)	2.10(2)
Mn(1)–O(6)	2.00(2)	Mn(2)–O(5)	2.24(2)
Mn(1)···Mn(2)	3.501(4)		
N(1)–Mn(1)–N(2)	77.2(8)	N(3)–Mn(2)–N(4)	76.8(9)
N(1)–Mn(1)–O(1)	94.2(7)	N(3)–Mn(2)–N(5)	87.6(8)
N(1)–Mn(1)–O(2)	84.4(8)	N(3)–Mn(2)–O(1)	99.9(8)
N(1)–Mn(1)–O(3)	168.7(8)	N(3)–Mn(2)–O(4)	166.4(9)
N(1)–Mn(1)–O(6)	84.1(9)	N(3)–Mn(2)–O(5)	81.9(7)
N(2)–Mn(1)–O(1)	148.4(7)	N(4)–Mn(2)–N(5)	91.1(8)
N(2)–Mn(1)–O(2)	91.9(7)	N(4)–Mn(2)–O(1)	176.4(7)
N(2)–Mn(1)–O(3)	93.0(8)	N(4)–Mn(2)–O(4)	91.9(8)
N(2)–Mn(1)–O(6)	97.1(8)	N(4)–Mn(2)–O(5)	86.1(8)
O(1)–Mn(1)–O(2)	56.8(6)	N(5)–Mn(2)–O(1)	87.2(7)
O(1)–Mn(1)–O(3)	97.1(7)	N(5)–Mn(2)–O(4)	100.3(8)
O(1)–Mn(1)–O(6)	112.4(7)	N(5)–Mn(2)–O(5)	169.6(7)
O(2)–Mn(1)–O(3)	101.8(8)	O(1)–Mn(2)–O(4)	91.6(7)
O(2)–Mn(1)–O(6)	163.5(8)	O(1)–Mn(2)–O(5)	94.9(7)
O(3)–Mn(1)–O(6)	91.5(9)	O(4)–Mn(2)–O(5)	89.9(7)

benzoate groups, and N(5) of the isothiocyanate group. The Mn–N and Mn–O bond distances fall in the smaller range of 2.10(2)–2.35(3) Å. The Mn(1)···Mn(2) intermetallic separation is 3.501(4) Å. The aromatic ring of the asymmetrically bridging benzoate group is in a stacking mode with the aromatic ring of baib and the ring–ring separation is ≈3.55–3.68 Å.

$[Co_2(baib)(O_2CMe)_3]BPh_4$ 3. An ORTEP drawing of complex **3** is shown in Fig. 2 together with the numbering scheme. The relevant bond distances and angles are given in Table 3.

The pair of cobalt ions are bridged by three acetate groups in the $\eta^1{:}\eta^1$ mode and the Co(1)···Co(2) intermetallic separation is 3.449(2) Å. The geometry about Co(1) is best depicted as a trigonal bipyramid with the articular nitrogen N(1) of one pendant arm and one acetate oxygen O(5) at the axial sites and the terminal nitrogen N(2) of the pendant arm and two acetate oxygens O(1) and O(3) in the equatorial plane; the N(1)–Co(1)–O(5) angle is 169.8(3)° and the sum of the O(1)–Co(1)–O(3), O(1)–Co(1)–N(2) and O(3)–Co(1)–N(2) angles is 359.5°. The geometry about Co(2) is similarly trigonal bipyramidal. The articular nitrogen N(3) of the other pendant arm and an acetate oxygen O(6) reside at the axial sites [N(3)–Co(2)–O(6) angle 170.1°] and the terminal nitrogen N(4) of the pendant arm and two acetate oxygens O(2) and O(4) reside in the equatorial plane [sum of O(2)–Co(1)–O(4),

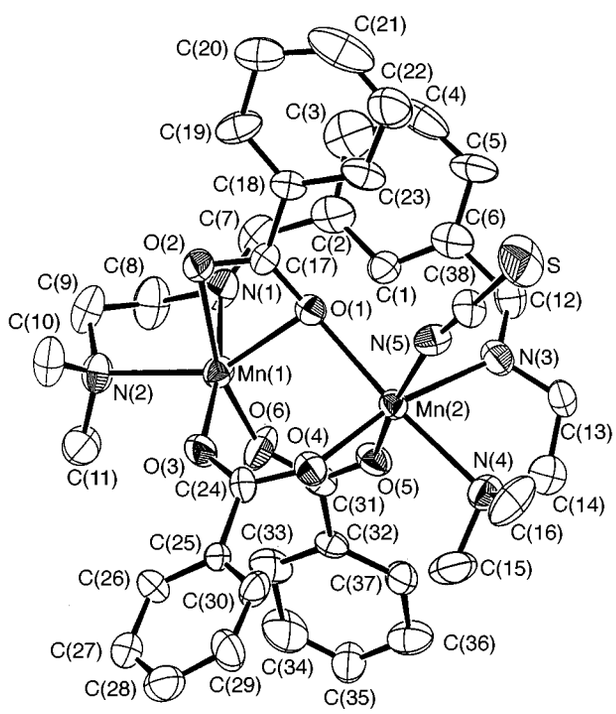

Fig. 1 An ORTEP drawing of the essential part of complex **2′** with the numbering scheme

O(2)–Co(1)–N(4) and O(4)–Co(1)–N(4) angles: 359.5°]. Two cobalt ions are not equivalent and Co(1) has short metal-to-ligand bonds (average 2.036 Å) relative to those of Co(2) (average 2.038 Å). The two equatorial planes about Co(1) and Co(2) are tilted at 136.61° to each other. Two bridging acetate groups form a near coplane and the third is nearly perpendicular to this coplane. The aromatic ring of baib is tilted 80.02° to the coplane formed by the two acetate bridges.

$[Co_2(baib)(O_2CPh)_3]BPh_4$·MeCN 4′. An ORTEP drawing of the cationic part of complex **4′** is shown in Fig. 3. This complex has a tri(μ-carboxylato)dicobalt(II) core very similar to that of **3** but some substantial geometrical differences are seen between **3** and **4′**. The Co(1)···Co(2) intermetallic separation of **4′** is 3.482(2) Å, slightly larger than that of **3**. This elongation leads to an increase in the dihedral angle between the two equatorial planes of Co(1) and Co(2) (124.62°) and a slight decrease in the N(1)–Co(1)–O(5) and N(3)–Co(2)–O(6) angles (167.7 and 169.6°, respectively). Further, the benzene ring of baib is brought closer to the coplane formed by the two acetate

Table 3 Relevant bond distances (Å) and angles (°) for complex **3**

Co(1)–N(1)	2.175(9)	Co(2)–N(3)	2.18(1)
Co(1)–N(2)	2.066(9)	Co(2)–N(4)	2.095(9)
Co(1)–O(1)	1.950(7)	Co(2)–O(2)	1.968(7)
Co(1)–O(3)	1.981(8)	Co(2)–O(4)	1.941(8)
Co(1)–O(5)	2.011(8)	Co(2)–O(6)	2.003(9)
Co(1)···Co(2)	3.449(2)		
N(1)–Co(1)–N(2)	81.5(4)	N(3)–Co(2)–N(4)	81.7(4)
N(1)–Co(1)–O(1)	91.1(3)	N(3)–Co(2)–O(2)	89.4(4)
N(1)–Co(1)–O(3)	89.5(3)	N(3)–Co(2)–O(4)	90.0(4)
N(1)–Co(1)–O(5)	169.8(3)	N(3)–Co(2)–O(6)	170.1(4)
N(2)–Co(1)–O(1)	114.8(4)	N(4)–Co(2)–O(2)	112.0(4)
N(2)–Co(1)–O(3)	110.7(5)	N(4)–Co(2)–O(4)	107.8(4)
N(2)–Co(1)–O(5)	88.4(4)	N(4)–Co(2)–O(6)	88.4(4)
O(1)–Co(1)–O(3)	134.1(3)	O(2)–Co(2)–O(4)	139.7(3)
O(1)–Co(1)–O(5)	94.8(3)	O(2)–Co(2)–O(6)	94.2(4)
O(3)–Co(1)–O(5)	92.3(4)	O(4)–Co(2)–O(6)	93.2(4)

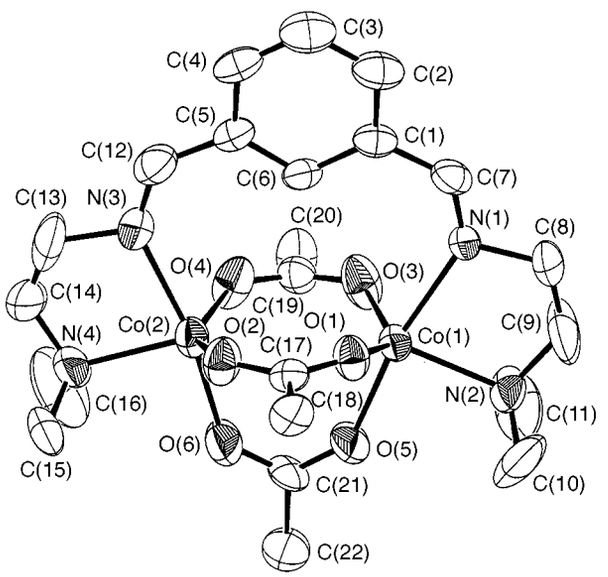

Fig. 2 An ORTEP drawing of the essential part of complex **3** with the numbering scheme

bridges, resulting in the enlarged dihedral angle between the benzene ring and the acetate-bridge coplane (73.3°). The cobalt-to-ligand bonds [average 2.045 Å for Co(1) and 2.055 Å for Co(2)] are elongated relative to those in **3**.

$[Zn_2(baib)(O_2CMe)_3]BPh_4$ 5. An ORTEP drawing of the cationic part of the complex is given in Fig. 4. The complex cation $[Zn_2(baib)(O_2CMe)_3]^+$ has a dinuclear core similar to that of **3**. The Zn(1)···Zn(2) intermetallic separation is 3.465(1) Å. Each Zn assumes a trigonal-bipyramidal geometry with an average metal-to-ligand bond length of 2.061 Å for Zn(1) and 2.059 Å for Zn(2). The zinc-to-ligand bond distances are long relative to the cobalt-to-ligand distances in **3** and **4**. The N(1)–Zn(1)–O(5) and N(3)–Zn(2)–O(6) angles are 170.0 and 170.8°, respectively. The dihedral angle between the aromatic ring of baib and the near coplane formed by the two acetate bridges is 84.28°.

Physicochemical properties

Magnetism. The magnetic moments of the manganese complexes **1** and **2** at room temperature are 5.66 and 5.75 μ_B, respectively, which decrease with decreasing temperature to 2.00 and 3.60 μ_B, respectively, near liquid-helium temperature. This strongly suggests the operation of antiferromagnetic spin exchange within each core. The temperature dependences of the magnetic susceptibility are shown in Fig. 5.

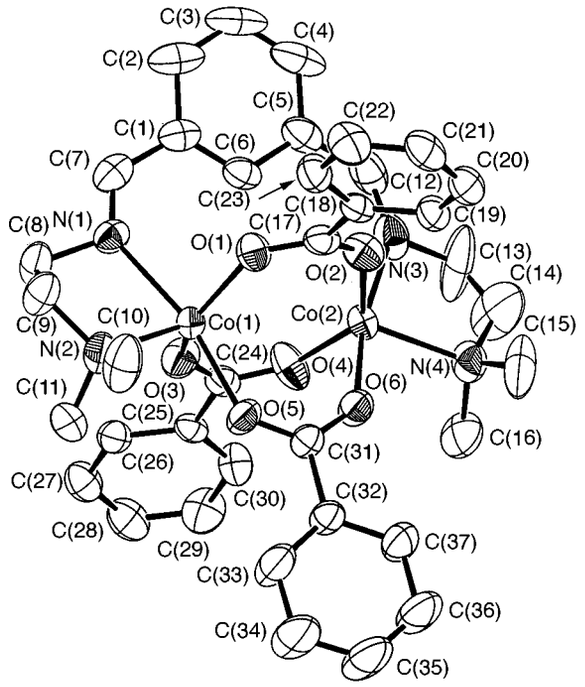

Fig. 3 An ORTEP drawing of the essential part of complex **4′** with the numbering scheme

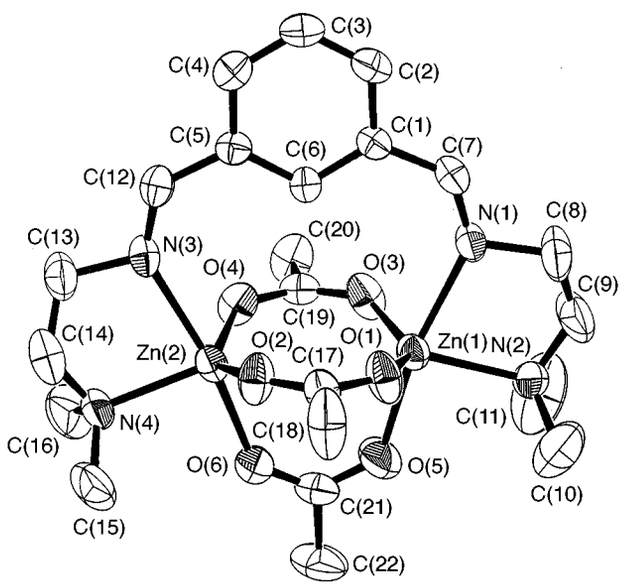

Fig. 4 An ORTEP drawing of the essential part of complex **5** with the numbering scheme

The magnetic susceptibility of complex **1** increases with decreasing temperature up to a maximum at 16 K then decreases below this temperature. The magnetic susceptibility for **2** tends to saturate near liquid-helium temperature. The cryomagnetic behaviour of the complexes can be reproduced by the magnetic susceptibility expression (1) for an $(S_1 = \frac{5}{2})$–$(S_2 = \frac{5}{2})$

$$\chi_A = [(Ng^2\beta^2/kT)(x^{28} + 5x^{24} + 14x^{18} + 30x^{10} + 55)/(x^{30} + 3x^{28} + 5x^{24} + 7x^{18} + 9x^{10} + 11)(1 - \rho)] + (35Ng^2\beta^2/12kT)\rho \quad (1)$$

system based on the isotropic Heisenberg model $H = -2JS_1S_2$.[17] In this equation $x = \exp(-J/kT)$, N is Avogadro's number, g the Zeeman splitting factor, β the Bohr magneton, k the Boltzmann constant, T the absolute temperature, J the exchange integral, and ρ the fraction of monomeric impurity. The temperature-independent paramagnetism for Mn^{II} is assumed to be zero. The best-fitting curves based on this

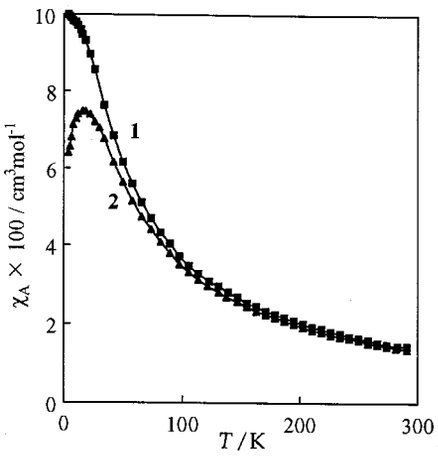

Fig. 5 The temperature dependences of magnetic susceptibility (per Mn) for complexes **1** and **2**

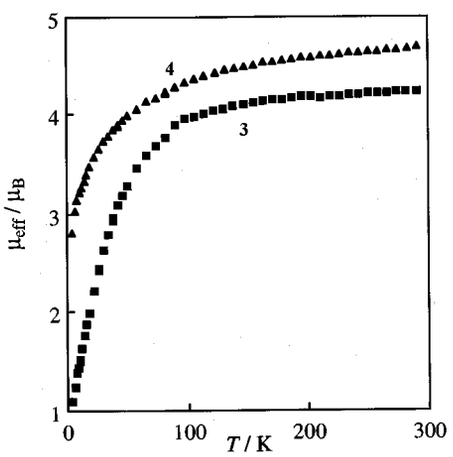

Fig. 6 The temperature dependences of the magnetic moment (per Co) for complexes **3** and **4**

equation are given by the solid lines in Fig. 5. The magnetic parameters obtained by this fitting and the discrepancy factor defined as $R(\mu) = [\Sigma(\mu_{obs} - \mu_{calc})^2/\Sigma(\mu_{obs})^2]^{\frac{1}{2}}$ are as follows: $g = 1.98$, $J = -2.10$, $\rho = 0$ and $R(\mu) = 4.7 \times 10^{-3}$ for **1** and $g = 1.99$, $J = -1.73$, $\rho = 0.023$ and $R(\mu) = 4.7 \times 10^{-3}$ for **2**. The results indicate the operation of an antiferromagnetic interaction within a pair of manganese(II) ions.

The room-temperature magnetic moments of the cobalt(II) complexes **3** and **4** are 4.2 and 4.7 μ_B, respectively, which decrease with decreasing temperature to 1.0 and 2.8 μ_B, respectively, at liquid-helium temperature (Fig. 6). Such cryomagnetic behaviour is indicative of antiferromagnetic interaction between the cobalt(II) ions but the μ_{eff} *vs.* T curves cannot be simulated by means of the magnetic susceptibility expression for a $(S_1 = \frac{3}{2})$–$(S_2 = \frac{3}{2})$ system based on the Heisenberg model. It is likely that a secondary effect substantially contributes to the magnetism of these complexes.

Spectroscopic properties. Absorption spectra were obtained in dmf or dichloromethane and numerical data are given in the Experimental section. The manganese complexes **1** and **2** are pale yellow and the zinc complex **5** is colourless. They show no prominent absorption in the visible region because Mn^{II} of high-spin d^5 electronic configuration has no spin-allowed d–d transition and Zn^{II} of d^{10} electronic configuration has no d–d transition. For **1** and **2** an intense absorption band is observed at ≈275 nm and two moderately intense bands at ≈296 and ≈306 nm (in dmf). The last two bands are also seen for free baib (295 and 306 nm) and thence can be attributed to intraligand transition bands. The intense band near 275 nm may be associated with a charge-transfer transition. The zinc complex **5** shows an intense absorption at 262 nm and a moderately intense absorption at 300 nm. An essentially similar ultraviolet spectrum is obtained for the cobalt complexes **3** and **4**.

The cobalt complexes are purple and their visible spectra in dichloromethane are characterized by three weak absorptions at ≈ 775, ≈556 and 480 nm, which are assigned to d–d transition bands of Co^{II} under D_{3h} symmetry.[18] Exactly the same visible spectrum was obtained when measured by reflection on a powdered sample, indicating the dinuclear core is retained in this solvent. In dmf solution the cobalt d–d bands are found at 500 and 520 nm.

Electrochemistry. The cyclic voltammograms of the manganese complexes **1** and **2** in dmf were irreversible; **1** showed three anodic peaks at +0.52, +0.85 and +1.20 V *vs.* $Ag–Ag^+$ and **2** showed two anodic peaks at +0.65 and +0.95 V. The anodic peak at +0.52 V of **1** is attributed to tetraphenylborate ion based on our comparative studies for $NaBPh_4$. The remaining two anodic peaks of **1** and the two peaks of **2** must be associated with the oxidation at the Mn. No prominent wave was observed for both complexes in the negative potential region.

The cyclic voltammograms of cobalt complexes **3** and **4** in dmf were not well resolved except for an anodic peak at ≈+0.75 V due to the tetraphenylborate ion. This peak was also observed for the zinc complex **5**. In dichloromethane **3** showed three anodic peaks at +0.58, +1.12 and +1.38 V (*vs.* $Ag–Ag^+$). The last two peaks at +1.12 and +1.38 V can be attributed to oxidation at Co. The high potential of the peaks means that the oxidation state Co^{II} is preferred to Co^{III} at the electrode. The stabilization of Co^{II} is evidently due to the trigonal-bipyramidal surroundings which are unfavourable for Co^{III} in view of the crystal-field stabilization energy. Complex **4** resembles **3** in electrochemical behaviour, showing three anodic peaks at +0.62, +1.28 and +1.42 V. No prominent wave was observed at available potentials for both **3** and **4** in the negative sweep.

CAT-like activity

The CAT-like activity of complexes **1**–**5** to disproportionate H_2O_2 into H_2O and O_2 was examined in dmf at 0 °C by volumetric measurements of evolved dioxygen and it was found that the manganese (**1** and **2**) and cobalt (**3** and **4**) complexes have such activity. The zinc complex **5** showed no activity.

Dinuclear manganese complexes (1 and 2). The time courses of oxygen evolution for the catalysis by complex **1** and **2** (2.5×10^{-3} M) are given in Fig. 7. In the catalysis by **1** the evolved dioxygen linearly increased first but tended to saturate after 50 min. Then more rapid evolution occurred after 70 min which ceased after 90 min. At this stage the evolved dioxygen corresponded to 100% decomposition of hydrogen peroxide. The evolution profile suggests the involvement of a slow catalytic process (A) occurring at the initial stage and a faster catalytic process (B) appearing after a lag time, though the saturation tendency of the slow catalysis is hardly explained. Complex **2** also showed a similar evolution profile where the fast catalytic process appeared after a longer lag time of *ca.* 150 min. The rates of the slow and the fast catalytic processes (v_a and v_b, respectively) and the lag time τ for the fast catalytic process were evaluated graphically as: $v_a = 5$, $v_b = 19$ μmol min^{-1} and $\tau = 60$ min for **1** and $v_a = 4$, $v_b = 20$ μmol min^{-1} and $\tau = 145$ min for **2**. When thiocyanate ion was added to the catalysis by **1** (complex : NCS^- = 1 : 1), the evolution profile was exactly the same as that for the catalysis by **2**. Evidently, thiocyanate ion acts as an inhibitor to the fast catalytic process (B). It must be emphasized that both v_a and v_b for the catalysis by **1** and **2** are small and the lag time τ is large relative to the catalysis by (μ-phenoxo)di(μ-carboxylato)dimanganese(II) complexes studied previously in our laboratory.[7]

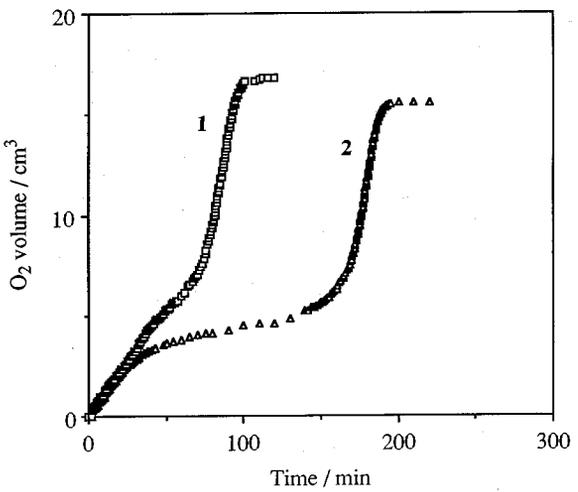

Fig. 7 Time courses of oxygen evolution in the disproportionation of H_2O_2 by complexes **1** and **2**. Conditions: 5 μmol complex in dmf (2 cm^3) containing H_2O_2 (10.0%, 0.5 cm^3) at 0 °C

In dmf both complexes act as 1:1 electrolytes, supporting the fact that the $[Mn_2(baib)(O_2CPh)_3]^+$ core persists in solution. The core has a five-co-ordinate Mn^{II} and its sixth vacant site is available for binding hydrogen peroxide. The bridge of hydrogen peroxide between two $[Mn_2(baib)(O_2CPh)_3]^+$ cores may lead to $Mn^{II}Mn^{III}(OH)$ species which can be involved in the slow catalytic process (A) through the interconversion of $Mn^{II}Mn^{III}(OH)/Mn^{II}Mn^{IV}(=O)$.[7] The involvement of a $Mn^{II}Mn^{III}$ mixed-valence species in the slow catalytic process has been demonstrated by ESR spectroscopy for macrocyclic dinuclear manganese complexes.[19,20]

The fast catalytic process is believed to employ a C_s symmetric dinuclear manganese core with an appropriate Mn···Mn separation to allow chelate bonding of H_2O_2 to the core.[7] To achieve such binding of H_2O_2 the $[Mn_2(baib)(O_2CPh)_3]^+$ core must release one of the acetate bridges to give $[Mn_2(baib)(O_2CPh)_2]^{2+}$ and this is related to the delayed appearance of the fast catalytic process (B) relative to the slow process (A). Added thiocyanate ion may co-ordinate to one of the manganese ions of $[Mn_2(baib)(O_2CPh)_2]^{2+}$ forming $[Mn_2(baib)(O_2CPh)_2(NCS)]^+$, and this explains the inhibiting function of the ion in the fast catalytic process (B).

In the fast catalysis by (μ-phenoxo)di(μ-carboxylato)-dimanganese(II) core complexes the involvement of $\{Mn^{IV}(=O)\}_2$ species has been evidenced by FAB mass spectrometry and visible spectroscopy.[7] The disproportionation of H_2O_2 by **1** has been examined by visible spectroscopy (Fig. 8). Just after the addition of H_2O_2 the solution was almost colourless and showed trace (*a*). When the fast catalytic process (B) started the solution became a purple colour and showed the spectrum (*b*). Of particular interest is the absorption band near 530 nm that has fine structures of *ca.* 730 cm^{-1} separation. This can be assigned to a ligand-to-metal charge-transfer (LMCT) band from oxo ion to Mn^{IV} and the fine structure is attributed to the ν(Mn=O) mode coupled to the LMCT band through vibronic interaction.[7] The result adds support to the conclusion that the fast catalytic process proceeds through the interconversion of *cis*-$\{Mn^{III}(OH)\}_2$ and *cis*-$\{Mn^{IV}(=O)\}_2$.[7] It must be mentioned that the oxygen evolution profile with **1** at 20 °C showed no lag period for the fast process and the absorption spectrum showed no characteristic band. This is because the catalytic cycle between *cis*-$\{Mn^{III}(OH)\}_2$ and *cis*-$\{Mn^{IV}(=O)\}_2$ becomes fast at elevated temperatures so that the *cis*-$\{Mn^{IV}(=O)\}_2$ species has a short lifetime and cannot be detected by visible spectroscopy.[19]

Dinuclear cobalt complexes (3 and 4). The complexes **3** and **4** showed a similar CAT-like activity. The catalytic function of **3** is described below. The time course of oxygen evolution is given in Fig. 9.

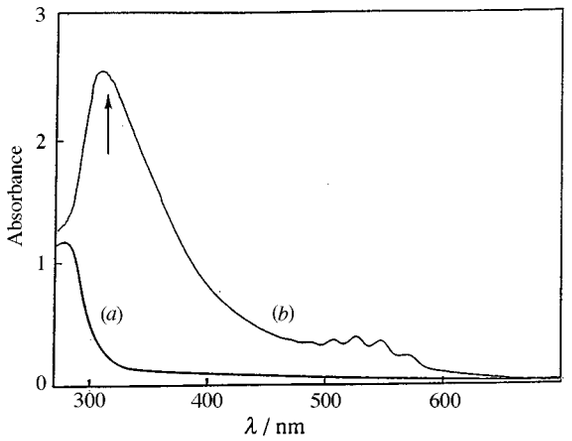

Fig. 8 Visible spectral changes in the disproportionation of H_2O_2 by complex **1** (under the conditions given in Fig. 7): (*a*) just after the addition of H_2O_2, (*b*) for the purple solution appearing after 170 min

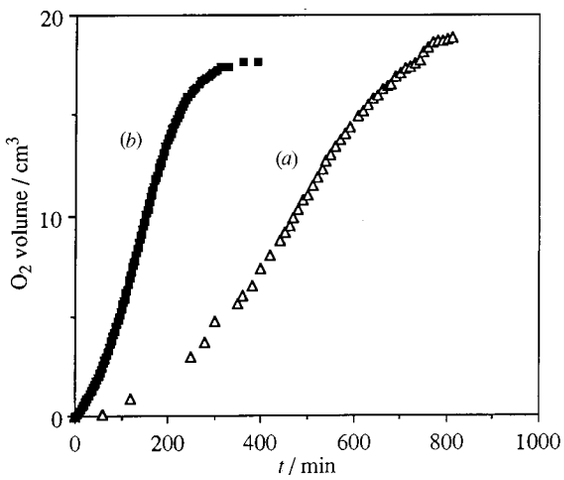

Fig. 9 The time course of oxygen evolution in the H_2O_2 disproportionation of H_2O_2 by complex **3** at the concentration of 2.5×10^{-3} M: (*a*) at 0 °C and (*b*) at 20 °C

When studied at 10 °C the oxygen evolution profile was sigmoidal and evolution ceased in 800 min. At this stage the evolved dioxygen corresponded to 100% decomposition of the added hydrogen peroxide. At 20 °C the catalysis became faster and the evolution ceased in 320 min. In the course of the catalysis at 10 °C the solution became brown and showed an intense absorption band at 365 nm and weaker bands at 560 and 650 nm. This suggests the involvement of Co^{III} in the catalysis. To the best of our knowledge this is the first cobalt complex to catalyse the disproportionation of hydrogen peroxide.

Acknowledgements

This work was supported by a Grant-in-Aid for Scientific Research (No. 09440231) from the Ministry of Education, Science and Culture, Japan.

References

1 D. E. Fenton and H. Ōkawa, *Perspectives on Bioinorganic Chemistry*, eds. R. W. Hay, J. R. Dilworth and K. B. Nolan, JAI Press, London, 1993, vol. 2, pp. 81–138.
2 M. A. Holms, I. LeTrong, S. Turkey, L. C. Sleker and R. E. Stenkamp, *J. Mol. Biol.*, 1991, **218**, 583.
3 P. Nordlund, B.-M. Sjoberg and H. Eklund, *Nature* (*London*), 1990, **345**, 593.

4 E. Hough, L. K. Hansen, B. Birknes, K. Jynge, S. Hansen, A. Hordvik, C. Little, E. J. Dodson and Z. Derewenda, *Nature* (*London*), 1989, **338**, 357.
5 K. Wieghardt, *Angew. Chem.*, *Int. Ed. Engl.*, 1989, **28**, 1153.
6 H. Sakiyama, H. Tamaki, M. Kodera, N. Matsumoto and H. Ōkawa, *J. Chem. Soc.*, *Dalton Trans.*, 1993, 591.
7 H. Sakiyama, H. Ōkawa and R. Isobe, *J. Chem. Soc.*, *Chem. Commun.*, 1993, 882; H. Sakiyama, H. Ōkawa and M. Suzuki, *J. Chem. Soc.*, *Dalton Trans.*, 1993, 3823.
8 C. Higuchi, H. Sakiyama, H. Ōkawa, R. Isobe and D. E. Fenton, *J. Chem. Soc.*, *Dalton Trans.*, 1994, 1097.
9 C. Higuchi, H. Sakiyama, H. Ōkawa and D. E. Fenton, *J. Chem. Soc.*, *Dalton Trans.*, 1995, 4015.
10 N. F. Curtis, *J. Chem. Soc.*, 1961, 3147.
11 E. A. Boudreaux and L. N. Mulay, *Theory and Applications of Molecular Paramagnetism*, Wiley, New York, 1976, pp. 491–494.
12 D. T. Cromer and J. T. Waber, *International Tables for X-Ray Crystallography*, Kynoch Press, Birmingham, 1974, vol. 4.
13 D. C. Creagh and W. J. McAuley, *International Tables for Crystallography*, Kluwer, Boston, 1992, vol. C, pp. 219–222.
14 D. C. Creagh and H. H. Hubbell, *International Tables for Crystallography*, Kluwer, Boston, 1992, vol. C, pp. 200–206.
15 TEXSAN, Molecular Structure Corporation, Houston, TX, 1985.
16 C. K. Johnson, ORTEP, Report 3794, Oak Ridge National Laboratory, Oak Ridge, TN, 1965.
17 P. W. Anderson, *Solid State Phys.*, 1963, **14**, 61; H. M. McConnell, *J. Chem. Phys.*, 1963, **39**, 1910.
18 L. Sacconi, M. Ciampolini and G. P. Speroni, *J. Am. Chem. Soc.*, 1965, **87**, 3102.
19 H. Wada, K. Motoda, M. Ohba, H. Sakiyama, N. Matsumoto and H. Ōkawa, *Bull. Chem. Soc. Jpn.*, 1995, **68**, 1105.
20 T. Aono, H. Wada, M. Yonemura, M. Ohba, H. Ōkawa and D. E. Fenton, *J. Chem. Soc.*, *Dalton Trans.*, 1997, 1527.

Received 3*rd June* 1997; *Paper* 7/03842I